Wear and Corrosion Properties of Cold-Sprayed AISI 316L Coatings Treated by Combined Plasma Carburizing and Nitriding at Low Temperature

Shinichiro Adachi * and **Nobuhiro Ueda**

Research Division of Metal Finishing and Analysis, Osaka Research Institute of Industrial Science and Technology, Ayumino 2-7-1, Izumi 594-1157, Japan; ueda@tri-osaka.jp
* Correspondence: shinadachi@tri-osaka.jp; Tel.: +81-725-51-2648; Fax: +81-725-51-2749

Abstract: Cold-sprayed AISI 316L stainless steel coatings are treated to form an austenite phase with excessive dissolved nitrogen (known as the S-phase) by plasma nitriding at temperatures below 450 °C. The S-phase is a hard and wear-resistant layer with high corrosion resistance. However, the S-phase layer formed after only nitriding is thin and the hardness abruptly decreases at a certain depth; it lacks mechanical reliability. We examined two types of combined low-temperature plasma treatment to enhance the mechanical reliability of the S-phase layer: (i) sequential and (ii) simultaneous. In the sequential plasma treatment, the carburizing step was followed by nitriding. In the simultaneous treatment, the nitriding and carburizing steps were conducted at the same time. Both combined plasma treatments succeeded in thickening the S-phase layers and changed the hardness depth profiles to decrease smoothly. In addition, anodic polarization measurements indicated that sequential treatment involving carburizing followed by nitriding for 2 h each resulted in high corrosion resistance.

Keywords: cold spray; plasma carburizing; plasma nitriding; wear resistance; corrosion resistance

1. Introduction

Conventional nitriding and carburizing for austenitic stainless steel plates at treatment temperatures over 500 °C improve the surface hardness, but reduce the corrosion resistance due to the formation of chromium nitride or carbide. In contrast, low-temperature nitriding and carburizing at temperatures below 450 °C for austenitic stainless steel plates can result in the formation of an austenite phase with excessive dissolved nitrogen known as the S-phase. The S-phase is not a nitride or carbide, but a solid solution of excessive nitrogen or carbon dissolved in the fcc lattice. The S-phase layers possess a high hardness and excellent wear resistance. Therefore, low-temperature nitriding and carburizing could be applied to austenitic stainless steel plates used under severe friction conditions. In addition, these treatments restrict the formation of chromium nitride or carbide, maintaining the corrosion resistance [1–17].

A few papers have been reported nitriding and nitrocarburizing for sprayed stainless steel coatings, including treatments at conventional and low-temperatures. For the conventional treatment, HVOF-sprayed stainless steel coating was treated by plasma nitriding and nitrocarburizing at the temperature of 550 °C has been reported by Park et al. [18]. In addition, Thomas Lindner reported that HVOF-sprayed stainless steel coating was treated by gas nitriding and nitrocarburizing at low temperatures [19,20]. Additionally, we examined plasma-sprayed AISI 316L stainless steel coatings that were treated by low-temperature treatments below 450 °C [21,22]. As a result, it was recognized that the plasma-sprayed stainless steel coatings had improved wear resistance, similar to steel plates.

However, plasma-sprayed stainless steel coatings include oxide layers, cracks, and pores in their structure, which deteriorate the corrosion resistance considerably.

Cold-spraying is not a fusing process but a solid particle stacking process. Hence, cold-sprayed coatings are without any oxides, similar to a bulk steel structure [23]. It was reported that thick cold-sprayed 316L stainless steel coatings show electrochemical polarization behavior similar to bulk stainless steels [24]. Therefore, it is expected that cold-sprayed AISI 316L coatings can be applied as corrosion protective coatings. Additionally, Villa et al. reported that cold-sprayed 316L coatings can be hardened by cold working during the deposition process, which can also result in increased strength, and the abrasive wear resistance of the coating is in the same order of magnitude as that of coatings produced by HVOF [25]. However, the hardness of the 316L coatings was 358 ± 36 HVN, which is insufficient to apply under severe wear conditions.

We have previously reported low-temperature plasma nitriding of cold-sprayed AISI 316L coatings to successfully improve the Vickers hardness to 1200 HV [26]. In particular, remelted AISI 316L coatings by a postlaser treatment had excellent corrosion protection for ordinary steel substrates due to a dense microstructure.

However, there is a concern that S-phase layers formed by nitriding without carburizing could be delaminated when an external force is applied, because the hardness of the S-phase layers declines drastically at a certain depth. Low-temperature treatments combining nitriding and carburizing have been reported to result in a milder hardness distribution (with hardness not declining drastically), excellent wear resistance, and thickening of the S-phase layers. There are two types of combined treatments—(i) sequential and (ii) simultaneous. In the sequential treatment, carburizing is followed by nitriding [27–29]. Meanwhile, in the simultaneous treatment, carburizing and nitriding are performed at the same time, using a gas mixture of carbon and nitrogen species [30–35]. We had previously examined combined low-temperature plasma treatments for plasma-sprayed AISI 316L coatings [36], consequently thick S-phase layers were produced by the simultaneous plasma treatment. In this paper, cold-sprayed AISI 316L coatings are applied simultaneously and sequentially combined with plasma nitriding and carburizing at temperatures ranging from 400 to 450 °C; we then examined the effects of the processes on the thickening of the S-phase layer, wear resistance, hardness depth distribution, and corrosion resistance.

2. Experimental Procedure

2.1. AISI 316L Coating by Cold-Spraying

The substrate was an ordinary steel plate (JIS: SS400) sized $25 \times 65 \times 6$ mm^3. The spraying material was AISI 316L stainless steel powder with diameter $16-45$ μm. The steel substrates were blasted by #36 alumina grit to roughen and remove the oxide layer as a pretreatment step before cold-spraying. Cold-spraying was performed with a PCS-1000 system (Plasma Giken Co., Ltd., Saitama, Japan) using helium as the propellant gas. The spraying was carried out with a helium gas pressure of 5 MPa, gas temperature of 950 °C, nozzle standoff distance from the substrate of 25 mm, and traverse speed of 300 mm s^{-1}. The thickness of the sprayed coatings was ~500 μm.

After spraying, the coatings were polished using metallographic 3-μm diamond paste to flatten and remove the surface layer. The final thicknesses of the sprayed coatings were over 200 μm.

The cross-section of the cold-sprayed AISI 316L coating was polished and observed using an optical microscope. The porosity of the cold-sprayed AISI 316L coating was measured using commercially available image analysis software with an image binarization for the coating's cross-sectional micrograph.

2.2. Combined Low-Temperature Plasma Carburizing and Nitriding Treatment

A laboratory-type DC plasma ion treatment machine (FECH-1N, Fuji Electronics Industry Co, Ltd., Osaka, Japan) was used for the low-temperature plasma treatments. The specimen was placed on a

holder in the chamber and the holder was connected to the cathode. The plasma gas mixtures for the carburizing and nitriding processes were CH_4:Ar:H_2 (5:50:45) and N_2:H_2 (80:20), respectively. The gas mixture for the simultaneous (nitrocarburizing) treatment was CH_4:N_2:H_2 (5:80:15). The treatment temperatures were 400, 425, and 450 °C and the total treatment time was 4 h (see Table 1).

2.3. Characterization of the S-phase

Cross-sectional micrographs were observed using an optical microscope. Samples were first etched with Marble's reagent (containing 20 mL HCl, 20 mL H_2O, and 4 g $CuSO_4$). In addition, the nitride layer thickness was measured at approximately 10 points per sample from the cross-sectional micrographs.

Table 1. Conditions of low-temperature plasma treatments at 400, 425 and 450 °C.

Symbol	Treatment	
Single Treatment		
C4 h	Carburizing 4 h	
N4 h	Nitriding 4 h	
Sequential Treatment		
	1st Treatment	2nd Treatment
C0.5 h→N3.5 h	Carburizing 0.5 h	Nitriding 3.5 h
C2 h→N2 h	Carburizing 2 h	Nitriding 2 h
Simultaneous Treatment		
(C+N)4 h	Nitrocarburizing 4 h	

X-ray diffraction measurements involving conventional θ–2θ scans were performed to evaluate the crystal structure using Rigaku Smart Lab (Tokyo, Japan) with Cu-Kα radiation generated at 40 kV and 150 mA.

The carbon and nitrogen depth distribution profiles were obtained glow-discharge optical emission spectroscopy (GDOES) on a Rigaku GDA750 system (Tokyo, Japan).

2.4. Wear Resistance

The surface hardness was measured with a Vickers tester (HMV-2000, Shimadzu Corporation, Kyoto, Japan) with a test load of 0.245 N. The Vickers test of each sample was repeated 8 times and the lowest and highest value were excluded.

The hardness depth profiles were measured by using a nanoindentation tester (ENT-1100a, Elionix, Tokyo, Japan) with a test load of 1 mN and the measurement was repeated 3 times.

The amount of specific wear was measured using a laboratory-type ball-on-disc reciprocal sliding wear tester, and it was performed under dry conditions. An Al_2O_3 ball (4.76 mm in diameter) was used in the tests at a sliding speed of 20 mm s^{-1}, frequency of 2 Hz, amplitude of 5 mm, sliding distance of 144 m, and load of 1.96 N. The wear test of each sample was repeated 3 times. The cross-sectional area of the wear trails was measured at 3 points by using a roughness meter, Mitutoyo Formtracer CS-5000 (Mitutoyo, Tokyo, Japan).

2.5. Corrosion Protection

The corrosion resistance was evaluated by electrochemical polarization measurements carried out using a potentiostat, HZ-5000 (Hokuto Denko Corporation, Tokyo, Japan), with an Ag/AgCl reference electrode and a platinum-plated counter electrode at a scan rate of 20 mV min^{-1} at 30 °C. The experiments were performed using 3.5 wt % NaCl solution, which was degassed by bubbling N_2 gas for at least 0.5 h before the measurement to eliminate the influence of dissolved oxygen. A voltage

of −0.7 V was applied to the sample for 600 s and the sample was then allowed to stand for 600 s before the polarization curve was measured.

After the measurements, the surface morphology was examined by optical microscopy.

3. Results and Discussion

3.1. S-phase Produced by Plasma Treatment

Figure 1 shows the cross-sectional microstructure of the as-sprayed AISI 316L coating, and the coating porosity was 1%.
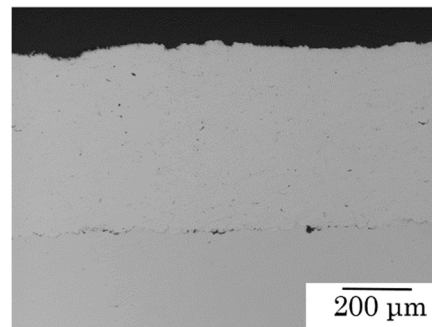

Figure 1. Cross-sectional micrograph of the cold-sprayed AISI 316L coating.

Figure 2 shows X-ray diffraction patterns of the sprayed AISI 316L coatings with and without the low-temperature plasma treatments. All XRD peaks for $\gamma(111)$ and $\gamma(200)$ were shifted towards lower angles by the plasma treatments, suggesting the γ-phase in the sprayed AISI 316L coatings expanded due to carbon and nitrogen atoms dissolving, indicating the formation of S-phase layers. In addition, at the treatment temperature of 450 °C, the small XRD peaks corresponding to Fe_3N and Cr_7C_3 were detected in the products of the combined plasma treatments and single carburizing treatment, respectively.
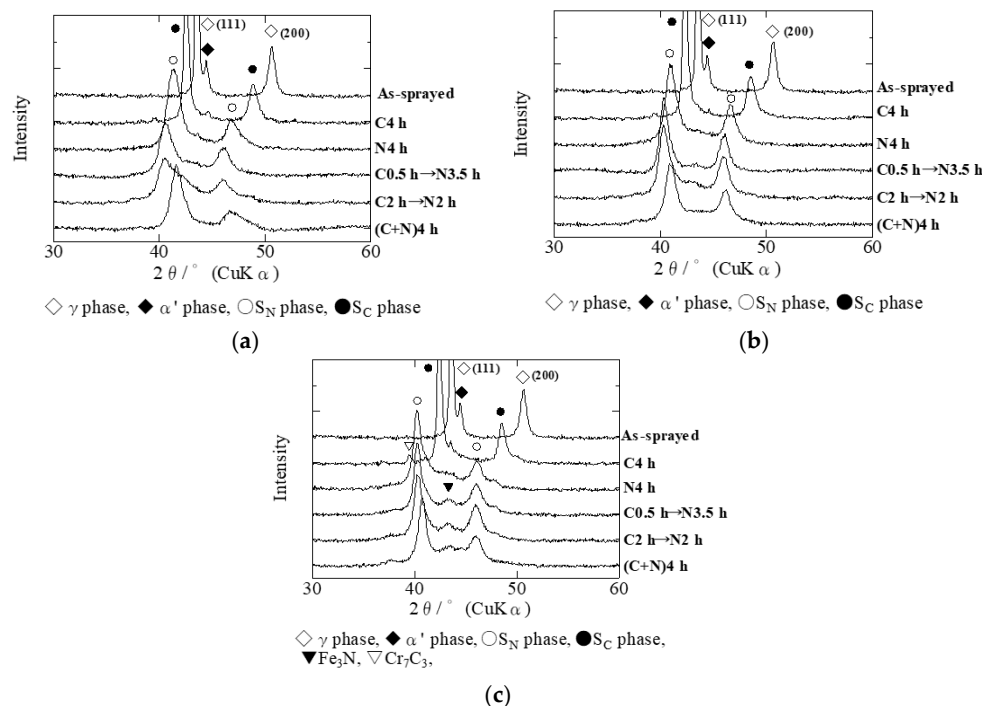

Figure 2. X-ray diffraction patterns of the cold-sprayed AISI 316L samples subjected to low-temperature plasma treatments at (**a**) 400 °C, (**b**) 425 °C and (**c**) 450 °C.

Cross-sectional micrographs for products obtained at the various treatments and temperatures are shown in Figures 3–5. The S-phase layers appear as the lighter region at the surface. The S-phase layers obtained with the combined plasma treatments were observed as a dual structure with a dark surface layer and a bright inner layer. Especially, at 450 °C, the dual structure was observed clearly. The carbon and nitrogen depth distributions obtained by GDOES are shown in Figure 6. For the combined plasma treatments, the GDOES results indicate that the nitrogen and carbon are present near the S-phase layer surface and inside, respectively. Then, it was concluded that the dark surface layer of the S-phase was rich in nitrogen (S_N-phase), and the inner bright layer was rich in carbon (S_C-phase).
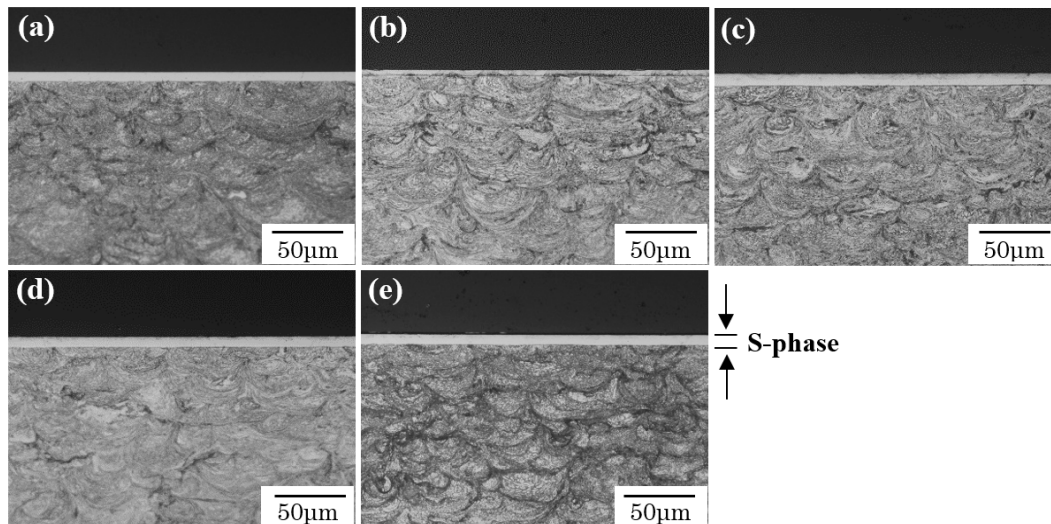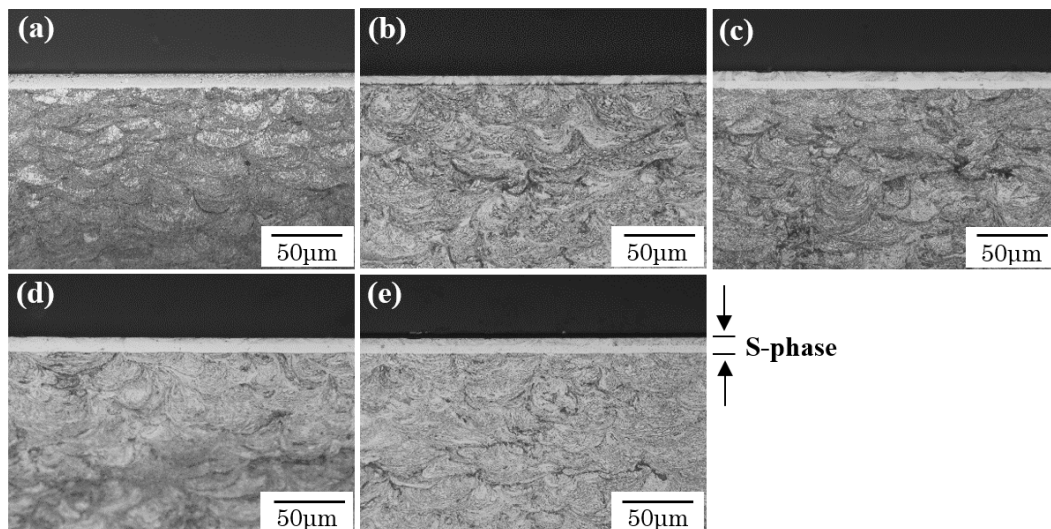

Figure 3. Cross-sectional micrographs of the S-phase layers on cold-sprayed AISI 316L coatings obtained at 400 °C by (**a**) carburizing for 4 h, (**b**) nitriding for 4 h, (**c**) C0.5 h→N3.5 h, (**d**) C2 h→N2 h, and (**e**) (C+N)4 h.
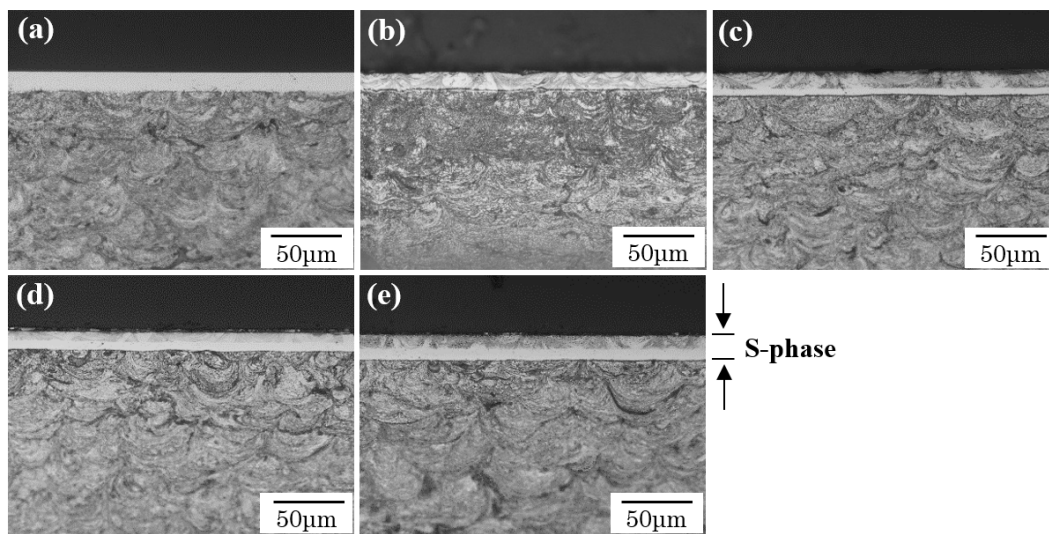

Figure 4. Cross-sectional micrographs of the S-phase layers on cold-sprayed AISI 316L coatings obtained at 425 °C by (**a**) carburizing for 4 h, (**b**) nitriding for 4 h, (**c**) C0.5 h→N3.5 h, (**d**) C2 h→N2 h, and (**e**) (C+N)4 h.

Figure 5. Cross-sectional micrographs of the S-phase layers on cold-sprayed AISI 316L coatings obtained at 450 °C by (**a**) carburizing for 4 h, (**b**) nitriding for 4 h, (**c**) C0.5 h→N3.5 h, (**d**) C2 h→N2 h, and (**e**) (C+N)4 h.
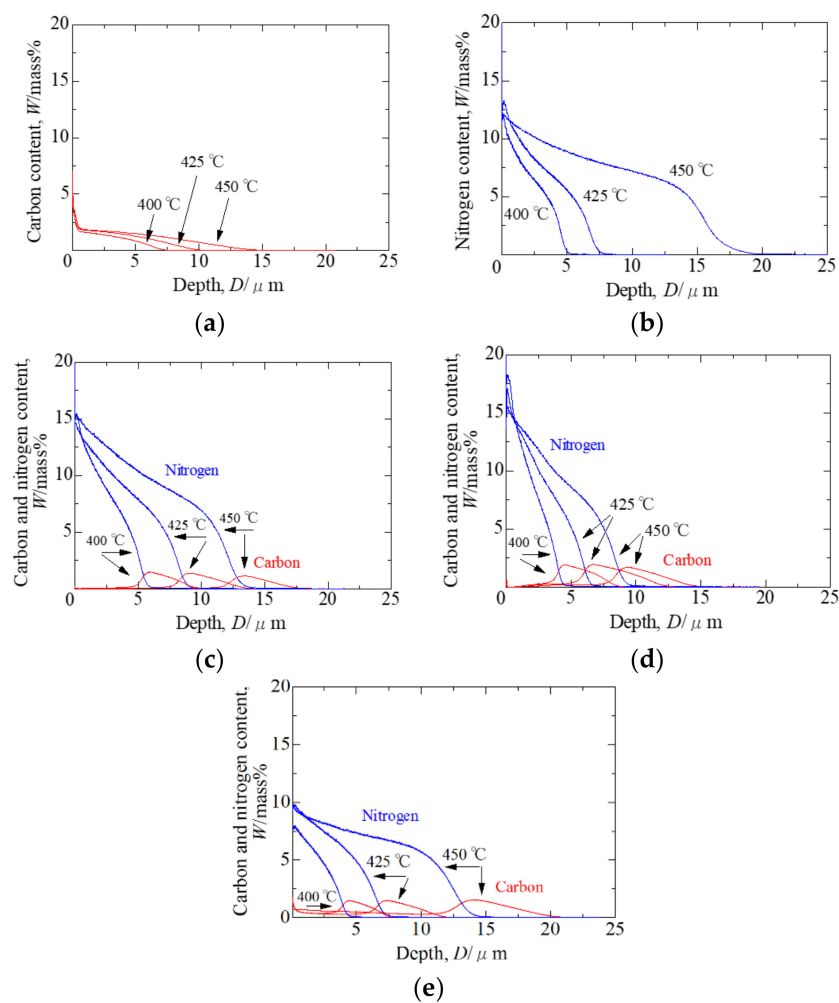

Figure 6. Carbon and nitrogen depth distributions of the S-phase layers on cold-sprayed AISI 316L coatings obtained at 400, 425 and 450 °C by (**a**) carburizing for 4 h, (**b**) nitriding for 4 h, (**c**) C0.5 h→N3.5 h, (**d**) C2 h→N2 h, and (**e**) (C+N)4 h.

The total thicknesses of the S-phase layers were measured from the cross-sectional micrographs and the values are shown in Figure 7. For the sequential plasma treatments, the average thicknesses of the (C0.5 h→N3.5 h) layers were 8.6 µm at 400 °C, 12.3 µm at 425 °C, and 16.7 µm at 450 °C. The (C2 h→N2 h) layer thicknesses were 7 µm at 400 °C, 10.7 µm at 425 °C, and 12.9 µm at 450 °C. Thus, the (C0.5 h→N3.5 h) layers were thicker than the (C2 h→N2 h) layers.
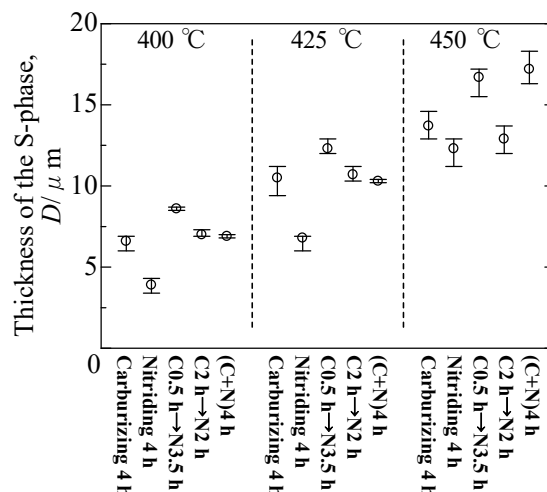

Figure 7. Thicknesses of the S-phase layers on cold-sprayed AISI 316L coatings subjected to various low-temperature plasma treatments at different temperatures.

From the GDOES results, in the (C2 h→N2 h) layer obtained at 450 °C (Figure 6d), the carbon-enriched layer was present at a depth of 9 µm from the surface. This depth was smaller compared to that of (C0.5 h→N3.5 h) obtained at 450 °C (13 µm, Figure 6c). The carburized layers of (C2 h→N2 h) formed during the first carburizing step are expected to restrict the nitrogen diffusion during the second nitriding step. In contrast, in (C0.5 h→N3.5 h), the carburized layers were pushed within easily by the second nitriding treatment, since the initial carburized layers were relatively thin due to the short treatment time of 0.5 h. Therefore, the S-phase layers of (C0.5 h→N3.5 h) are thicker than the (C2 h→N2 h) layers. In addition, the (C0.5 h→N3.5 h) layers were thicker than layers obtained by single treatment carburizing and nitriding. Consequently, the combination of the S_N-phase and S_C-phase would lead to the advantageous thickening of the S-phase layer.

Furthermore, in the XRD peaks of Figure 2, the peaks of products obtained by the sequential treatments (C0.5 h→N3.5 h) and (C2 h→N2 h) were shifted to lower angles than the peaks of the products obtained by single nitriding (N4 h) at 400 and 425 °C. The XRD peaks shifting to lower angles suggest more nitrogen dissolved in austenitic lattice. Consequently, the sequential plasma treatments enable the dissolution of higher nitrogen content compared to the single plasma treatments.

In simultaneous treatments ((C+N)4 h), as shown in Figure 5e, the S-phase layer was also a dual layer, similar to the sequential treatments. The GDOES results in Figure 6e suggest that the nitrogen concentration in S-phase layers obtained by simultaneous treatments was high at the surface and decreased in the interior. In contrast, the carbon concentration was relatively low at the surface and a carbon-enriched layer was formed at the inner side, where the nitrogen concentration decreased abruptly. The diffusion rate of carbon in austenite is faster than that of nitrogen [30], therefore carbon could penetrate ahead of nitrogen despite simultaneous carbon and nitrogen diffusion. Simultaneous treatment at 450 °C seemed to lead to lower Fe_3N formation compared to sequential treatments in Figure 2c. GDOES results in Figure 6e show that the simultaneous treatment resulted in a surface nitrogen concentration of 10 wt %, while the sequential treatments (Figure 6c,d) resulted in a concentration of 15 wt %. Further, the XRD profiles in Figure 2 suggest that the peak shifts of the γ-phase with the simultaneous treatments were less compared to that observed in sequential treatments. Consequently, the simultaneous treatments dissolved less nitrogen than the sequential treatments;

therefore, the simultaneous treatment at 450 °C lowered Fe$_3$N formation. In addition, the S-phase layers obtained with the simultaneous treatment at 400 °C and 425 °C were not thick compared to those obtained by single carburizing (C4 h); however, at 450 °C the simultaneous treatment resulted in a thick S-phase layer. Therefore, simultaneous treatment at 450 °C is suitable for cold-sprayed AISI 316L coatings to produce a thick S-phase layer with low Fe$_3$N content.

3.2. Hardness and Wear Resistance

The Vickers hardness and the specific wear of the as-sprayed 316L coatings were 370 HV and 6.4×10^{-14} m^2 N^{-1}, respectively. Figures 8 and 9 show the hardness and specific wear of the S-phase layers. For S-phase layers obtained by single carburizing (C4 h), the hardness was 800–1000 HV and the specific wear was ~1.5×10^{-14} m^2 N^{-1} at all treatment temperatures. In comparison with other plasma treatments, single carburizing led to inferior wear resistance.
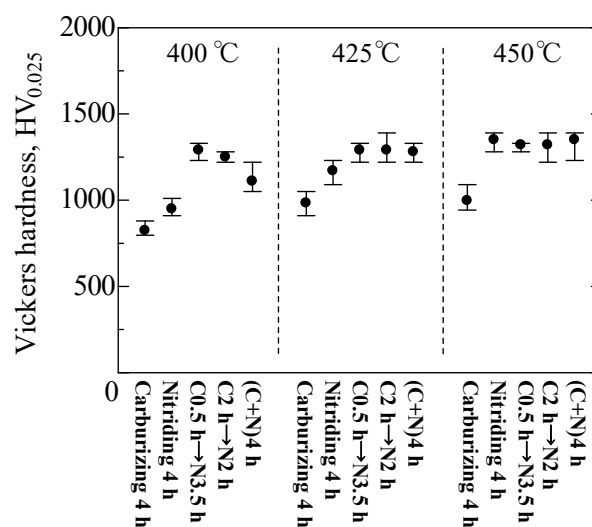
Figure 8. Hardness of the S-phase layers on cold-sprayed AISI 316L coatings subjected to various low-temperature plasma treatments at different temperatures.
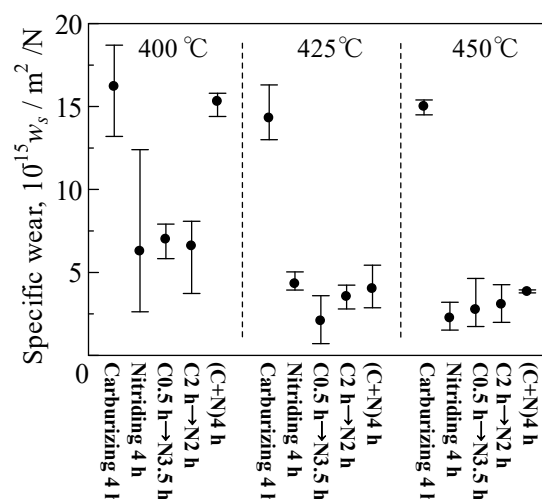
Figure 9. Specific wear of the S-phase layers on cold-sprayed AISI 316L coatings obtained by various low-temperature plasma treatments at different temperatures.

S-phase layers obtained by single nitriding (N4 h) showed a maximum hardness of 1350 HV at 450 °C and the sequential and simultaneous treatments at 450 °C also led to similar hardness values. On the other hand, at 400 and 425 °C, single nitriding led to lower hardness values than the combined

plasma treatments. The low hardness resulting from the single nitriding could be due to the thin S-phase layer formed (Figure 7), and therefore, the unmodified AISI 316L coating layer under the S-phase could affect the hardness.

On the other hand, the average amounts of specific wear of products obtained at 425 and 450 °C by single nitriding, sequential, and simultaneous treatments were in the range of $1–5 \times 10^{-15}$ m^2 N^{-1}. The S-phase layers obtained by the combined plasma treatments were composed of a surface S_N-phase and an interior S_C-phase; therefore, the properties of the wear resistance would not be very different in comparison to S-phase layers obtained by single nitriding treatment.

Figure 10a shows the nanoindentation hardness-depth profiles of the S-phase layers by the single plasma treatments obtained at 450 °C. The coating hardness after single nitriding (N4 h) decreased abruptly at a depth of 10 to 14 μm. Meanwhile, the hardness of S-phase layers obtained by single carburizing (C4 h) decreased gradually from the surface to the inside; however, these samples show a low hardness compared to the other plasma treatments.
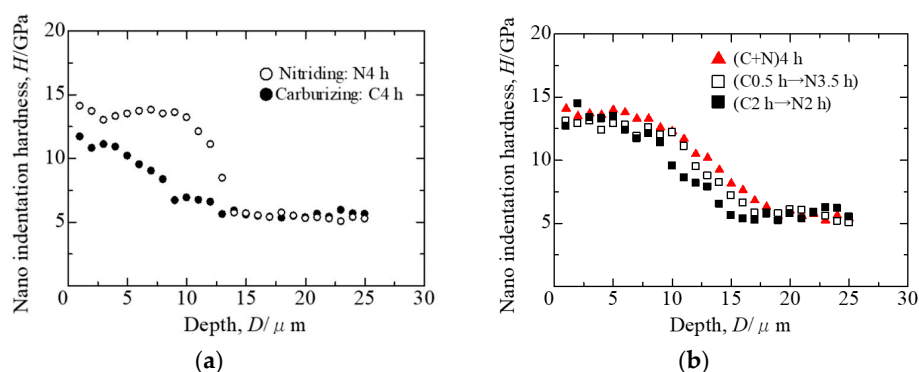

Figure 10. Hardness depth profiles of the S-phase layers on cold-sprayed AISI 316L coatings obtained at 450 °C by (**a**) single carburizing and nitriding treatments and (**b**) combined plasma treatments.

For S-phase layers obtained by the combined plasma treatments, the hardness (Figure 10b) decreased gradually at depths of 10 to 15 μm. In addition, the surface hardness was almost the same as those by single nitriding (N4 h), because the S-phase layers obtained with the combined plasma treatments were composed of the surface S_N-phase. The hardness distribution of samples obtained with sequential plasma treatment of (C0.5 h→N3.5 h) and simultaneous treatment of ((C+N)4 h) showed higher hardness profiles than those obtained by single nitriding (N4 h). Meanwhile, the sequential plasma treatment of (C2 h→N2 h) led to low hardness in samples at depths over 10 μm. The GDOES results in Figure 6d suggest that the nitrogen content of samples subjected to (C2 h→N2 h) at 450 °C decreased at a depth of 8 μm, conversely carbon content increased; therefore, the hardness of S-phase layers obtained by (C2 h→N2 h) are close to the hardness of samples obtained by single carburizing (C4 h).

Consequently, combined plasma processes including the sequential treatment of (C0.5 h→N3.5 h) and simultaneous treatment of ((C+N)4 h) improved the hardness depth distribution of S-phase layers of cold-sprayed AISI 316L coatings.

3.3. Corrosion Resistance

Figure 11 shows the anodic polarization curves of the S-phase layers obtained by single carburizing and nitriding at various treatment temperatures. Figure 12 shows the corresponding results of sequence and simultaneous plasma treated samples. All current densities of the S-phase layers at over ~0.2 V were lower than the as-sprayed AISI 316L coatings. Figure 13 shows the surface morphologies after the anodic polarization measurement. The as-sprayed AISI 316L coating clearly showed pitting corrosion; in contrast, the S-phase layers only changed colors at the surface with only a few sites of pitting corrosion. These indicate that low-temperature plasma treatments of sprayed AISI 316L coatings enhanced corrosion resistance by inhibiting the pitting corrosion.
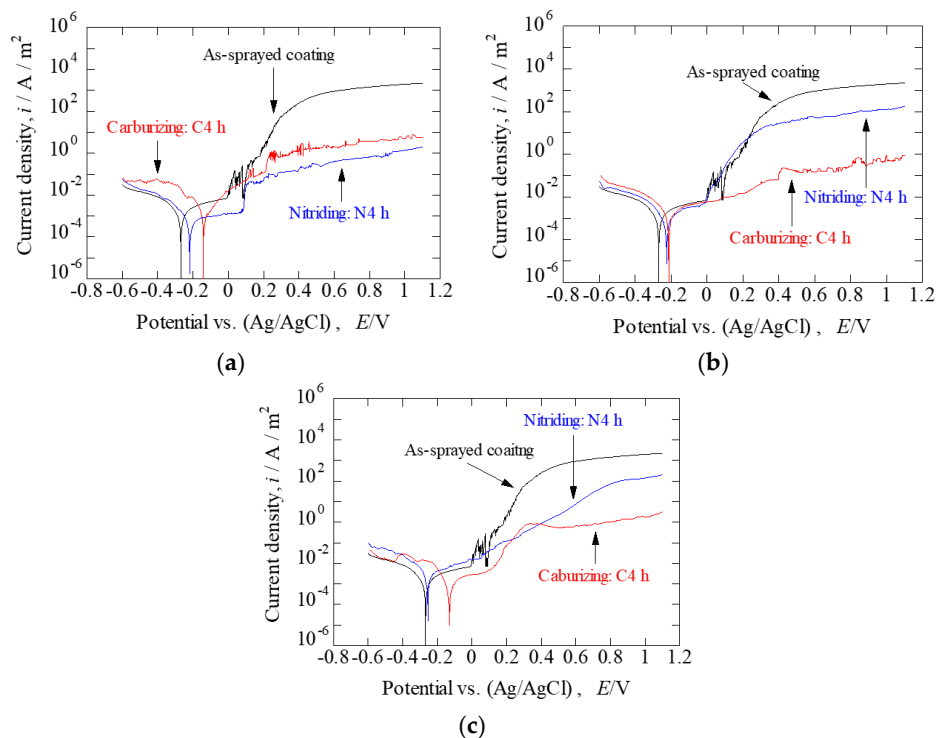
Figure 11. Anodic polarization curves in 3.5 wt % NaCl solution of the S-phase layers on cold-sprayed AISI 316L coatings obtained by 4 h carburizing and 4 h nitriding at (**a**) 400 °C, (**b**) 425 °C and (**c**) 450 °C.
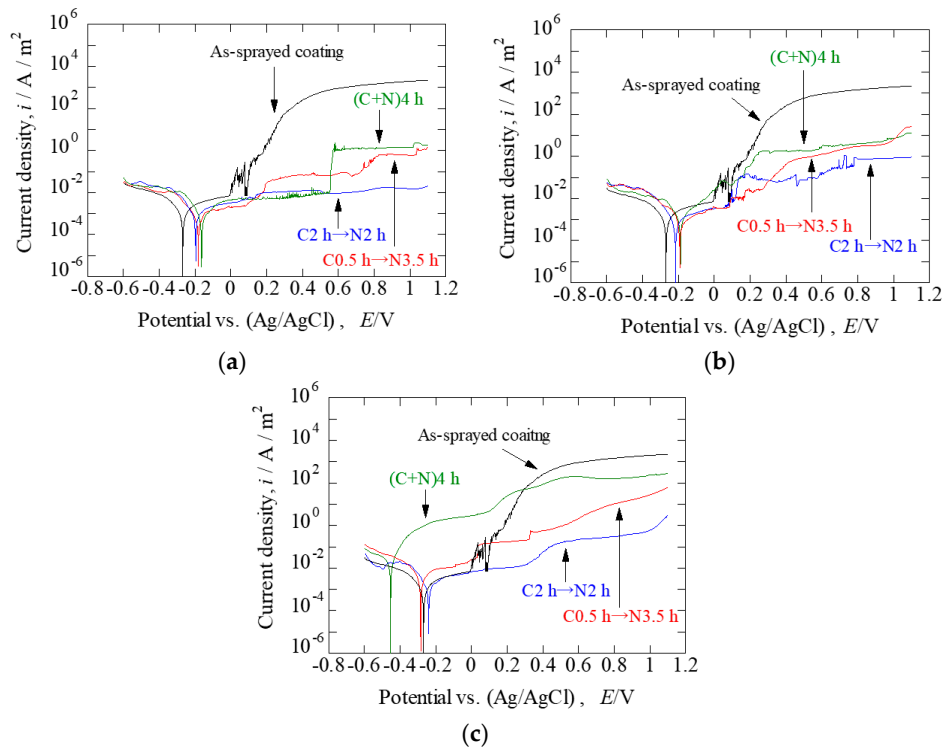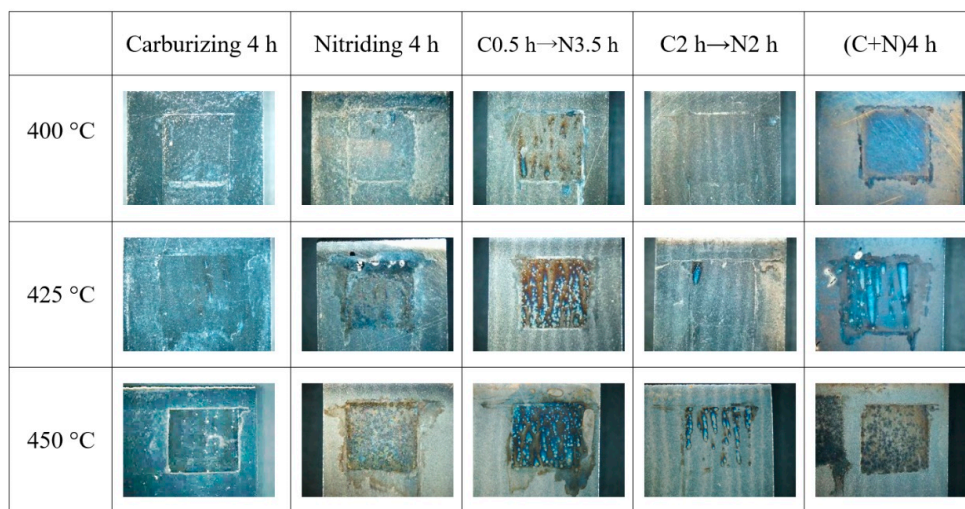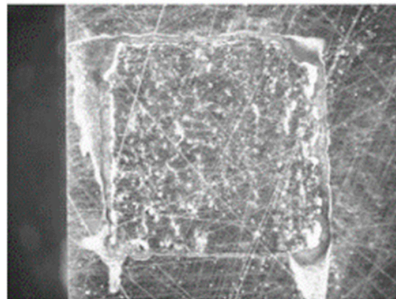

Figure 12. Anodic polarization curves in 3.5 wt % NaCl solution of S-phase layers on cold-sprayed AISI 316L coatings obtained by (C0.5 h→N3.5 h), (C2 h→N2 h) and ((C+N)4 h) at (**a**) 400 °C, (**b**) 425 °C and (**c**) 450 °C.

	Carburizing 4 h	Nitriding 4 h	C0.5 h→N3.5 h	C2 h→N2 h	(C+N)4 h
400 °C					
425 °C					
450 °C					

(**a**)

(**b**)

Figure 13. Surface morphology after anodic polarization measurements of (**a**) the S-phase layers on cold-sprayed AISI 316L coatings subjected to various low-temperature plasma treatments at different temperatures and (**b**) as-sprayed AISI 316L coating.

The effect of treatment temperatures on the corrosion resistance indicates that S-phase layers obtained at 400 °C show lower current density and corrosion-inhibiting surface morphology than samples obtained at 425 and 450 °C. The excellent corrosion resistance of samples treated at 400 °C is attributed to suppressed Fe_3N formation (Figure 2) as Fe_3N deteriorates corrosion resistance severely [31,37]. In addition, the (C2 h→N2 h) also led to excellent corrosion resistance among the combined plasma treatments. However, it is unclear why the S-phase layers with (C2 h→N2 h) enhanced corrosion resistance. The possibility of nitrogen and carbon supersaturation in austenite is reported to improve the passivation ability with an increase in the degree of supersaturation [31]. The S-phase layers with (C2 h→N2 h) showed the highest surface nitrogen content among the plasma treated samples (Figure 6); therefore, the surface layers obtained with (C2 h→N 2 h) would show high passivation ability. In addition, in comparison to single carburizing and nitriding treatments, the S-phase layer obtained with (C2 h→N2 h) at 400 °C showed lower corrosion current density, and those obtained at 425 and 450 °C also demonstrated marginally advantageous corrosion resistance behaviors. Therefore, sequential plasma treatment (C2 h→N2 h), especially at 400 °C, was most effective for enhancing the corrosion resistance of cold-sprayed AISI 316L coatings.

4. Conclusions

Low-temperature plasma carburizing, nitriding, and combined carburizing and nitriding were carried out on cold-sprayed AISI 316L coatings to improve the wear resistance. The combined treatments led to thicker S-phase layers than the single nitriding treatment. The wear resistance of the combined treatments was nearly identical to that of the single nitriding treatment. The hardness depth profiles

of samples obtained by single nitriding decreased abruptly at a certain depth, while those of samples obtained by combined treatments decreased gradually. Hence, combined treatment of cold-sprayed AISI 316L coatings enhanced the wear resistance and resulted in high mechanical reliability under external load. In particular, the S-phase obtained by sequential treatment (C0.5 h→N3.5 h) was a thick and superior wear resistant layer, irrespective of treatment temperature.

In contrast, the sequential treatment (C2 h→N2 h) led to inferior hardness depth profiles than that obtained by single nitriding and the other combined plasma treatments. However, the S-phase layers obtained with (C2 h→N2 h) showed a small corrosion current density and corroded only slightly after the anode polarization measurement. Consequently, the S-phase layers with (C2 h→N2 h) are suitable to be applied under corrosive environment.

Author Contributions: Conceptualization, S.A. and N.U.; Methodology, S.A. and N.U.; Investigation, S.A. and N.U.; Resources, S.A.; Data Curation, S.A.; Writing-Original Draft Preparation, S.A.; Writing-Review & Editing, S.A.; Visualization, S.A.; Supervision, N.U.; Project Administration, S.A.; Funding Acquisition, S.A.

Conflicts of Interest: The authors declare no conflicts of interest.

References

1. Zhang, Z.L.; Bell, T. Structure and Corrosion Resistance of Plasma Nitride Stainless Steel. *Surf. Eng.* **1985**, *1*, 131–136. [CrossRef]
2. Ichii, K.; Fujimura, K.; Takase, T. Structure of the Ion-Nitrided Layer of 18-8 Stainless Steel. *Tech. Rep. Kansai Univ.* **1986**, *27*, 135–144. (In Japanese)
3. Saker, A.; Leroy, C.; Michel, H.; Frantz, C. Properties of Sputtered Stainless Steel-Nitrogen Coatings and Structural Analogy with Low Temperature Plasma Nitrided Layers of Austenitic Steels. *Mater. Sci. Eng. A* **1990**, *140*, 702–708. [CrossRef]
4. Menthe, E.; Rie, K.-T.; Schultze, J.W.; Simson, S. Structure and Properties of Plasma Nitrided Stainless Steel. *Surf. Coat. Technol.* **1995**, *74*, 412–416. [CrossRef]
5. Larisch, B.; Brusky, U.; Spies, H.-J. Plasma Nitriding of Stainless Steels at Low Temperatures. *Surf. Coat. Technol.* **1999**, *116*, 205–211. [CrossRef]
6. Sun, Y.; Li, X.Y.; Bell, T. X-ray Diffraction Characterization of Low Temperature Plasma Nitrided Austenitic Stainless Steels. *J. Mater. Sci.* **1999**, *34*, 4793–4802. [CrossRef]
7. Liang, W.; Bin, X.; Zhiwei, Y.; Yaqin, S. The Wear and Corrosion Properties of Stainless Steel Nitride by Low-Pressure Plasma-Arc Source Ion Nitriding at Low Temperatures. *Surf. Coat. Technol.* **2000**, *130*, 304–308. [CrossRef]
8. Baranow, J. Characteristic of the Nitride Layers on the Stainless Steel at Low Temperature. *Surf. Coat. Technol.* **2004**, *180*, 145–149. [CrossRef]
9. Mingolo, N.; Tschiptschin, A.P.; Pinedo, C.E. On the Formation of Expanded Austenite During Plasma Nitriding of an AISI 316L Austenitic Stainless Steel. *Surf. Coat. Technol.* **2006**, *201*, 4215–4218. [CrossRef]
10. Gontijo, L.C.; Machado, R.; Miola, E.J.; Casteletti, L.C.; Alcantara, N.G.; Nascente, P.A.P. Study of the S phase formed on plasma-nitrided AISI 316L stainless steel. *Mater. Sci. Eng. A* **2006**, *431*, 315–321. [CrossRef]
11. Hamdy, A.S.; Marx, B.; Butt, D. Corrosion Behavior of Nitride Layer Obtained on AISI 316L Stainless Steel Via Simple Direct Nitridation Route at Low Temperature. *Mater. Chem. Phys.* **2011**, *126*, 507–514. [CrossRef]
12. Chemkhi, M.; Retraint, D.; Roos, A.; Garnier, C.; Waltz, L.; Demangel, C.; Proust, G. The Effect of Surface Mechanical Attrition Treatment on Low Temperature Plasma Nitriding of an Austenitic Stainless Steel. *Surf. Coat. Technol.* **2013**, *221*, 191–195. [CrossRef]
13. Köster, K.; Kaestner, P.; Bräuer, G.; Hoche, H.; Troßmann, T.; Oechsner, M. Material Condition Tailored to Plasma Nitriding Process for Ensuring Corrosion and Wear Resistance of Austenitic Stainless Steel. *Surf. Coat. Technol.* **2013**, *228*, S615–S618. [CrossRef]
14. Stinville, J.C.; Cormier, J.; Templier, C.; Villechaise, P. Monotonic Mechanical Properties of Plasma Nitride 316L Polycrystalline Austenitic Stainless Steel: Mechanical Behavior of the Nitride Layer and Impact of Nitriding Residual Stresses. *Mater. Sci. Eng. A* **2014**, *605*, 51–58. [CrossRef]

15. Borgioli, F.; Galvanetto, E.; Bacci, T. Low Temperature Nitriding of AISI 300 and 200 Series Austenitic Stainless Steels. *Vacuum* **2016**, *127*, 51–60. [CrossRef]

16. Zhao, G.-H.; Aune, R.E.; Espallargas, N. Tribocorrosion Studies of Metallic Biomaterials: The Effect of Plasma Nitriding and DLC Surface Modifications. *J. Mech. Behav. Biomed. Mater.* **2016**, *63*, 100–114. [CrossRef]

17. Yang, W.J.; Zhang, M.; Zhao, Y.H.; Shen, M.L.; Lei, H.; Xu, L.; Xiao, J.Q.; Gong, J.; Yu, B.H.; Sun, C. Enhancement of Mechanical Property and Corrosion Resistance of 316 L Stainless Steels by Low Temperature Arc Plasma Nitriding. *Surf. Coat. Technol.* **2016**, *298*, 64–72. [CrossRef]

18. Park, G.; Bae, G.; Moon, K.; Lee, C. Effect of Plasma Nitriding and Nitrocarburizing on HVOF-Sprayed Stainless Steel Coatings. *J. Therm. Spray Technol.* **2013**, *22*, 1366–1373. [CrossRef]

19. Lindner, T.; Mehner, T.; Lampke, T. Surface modification of austenitic thermal-spray coatings by low-temperature nitrocarburizing. *IOP Conf. Series Mater. Sci. Eng.* **2016**, *118*, 012008. [CrossRef]

20. Lindner, T.; Kutschmann, P.; Löbel, M.; Lampke, T. Hardening of HVOF-Sprayed Austenitic Stainless-Steel Coatings by Gas Nitriding. *Coatings* **2018**, *8*, 348. [CrossRef]

21. Adachi, S.; Ueda, N. Formation of S-phase layer on plasma sprayed AISI 316L stainless steel coating by plasma nitriding at low temperature. *Thin Solid Films* **2012**, *523*, 11–14. [CrossRef]

22. Adachi, S.; Ueda, N. Surface hardness improvement of plasma-sprayed AISI 316L stainless steel coating by low-temperature plasma carburizing. *Adv. Powder Technol.* **2013**, *24*, 818–823. [CrossRef]

23. Adachi, S.; Ueda, N. Effect of Cold-Spray Conditions Using a Nitrogen Propellant Gas on AISI 316L Stainless Steel-Coating Microstructures. *Coatings* **2017**, *7*, 87. [CrossRef]

24. Spencer, K.; Zhang, M.-X. Optimisation of stainless steel cold spray coatings using mixed particle size distributions. *Surf. Coat. Technol.* **2011**, *205*, 5135–5140. [CrossRef]

25. Villa, M.; Dosta, S.; Guilemany, J.M. Optimization of 316L stainless steel coatings on light alloys using Cold Gas Spray. *Surf. Coat. Technol.* **2013**, *235*, 220–225. [CrossRef]

26. Adachi, S.; Ueda, N. Formation of Expanded Austenite on a Cold-Sprayed AISI 316L Coating by Low-Temperature Plasma Nitriding. *J. Therm. Spray Technol.* **2015**, *24*, 1399–1407. [CrossRef]

27. Tsujikawa, M.; Yamauchi, N.; Ueda, N.; Sone, T.; Hirose, Y. Behavior of Carbon in Low temperature Plasma Nitriding Layer of Austenitic Stainless Steel. *Surf. Coat. Technol.* **2005**, *193*, 309–313. [CrossRef]

28. Tsujikawa, M.; Yoshida, D.; Yamauchi, N.; Ueda, N.; Sone, T.; Tanaka, S. Surface Material Design of 316 Stainless Steel by Combination of Low Temperature Carburizing and Nitriding. *Surf. Coat. Technol.* **2005**, *200*, 507–511. [CrossRef]

29. Sun, Y.; Haruman, E. Effect of Carbon Addition on Low-Temperature Plasma Nitriding Characteristics of Austenitic Stainless Steel. *Vacuum* **2006**, *81*, 114–119. [CrossRef]

30. Sun, Y. Hybrid Plasma Surface Alloying of Austenitic Stainless Steels with Nitrogen and Carbon. *Mater. Sci. Eng. A* **2005**, *404*, 124–129. [CrossRef]

31. Sun, Y. Enhancement in Corrosion Resistance of Austenitic Stainless Steels by Surface Alloying with Nitrogen and Carbon. *Mater. Lett.* **2005**, *59*, 3410–3413. [CrossRef]

32. Cheng, Z.; Li, C.X.; Dong, H.; Bell, T. Low Temperature Plasma Nitrocarburising of AISI 316 Austenitic Stainless Steel. *Surf. Coat. Technol.* **2005**, *191*, 195–200. [CrossRef]

33. Sun, Y.; Haruman, E. Influence of Processing Conditions on Structural Characteristics of Hybrid Plasma Surface Alloyed Austenitic Stainless Steel. *Surf. Coat. Technol.* **2008**, *202*, 4069–4075. [CrossRef]

34. Anjos, A.D.; Scheuer, C.J.; Brunatto, S.F.; Cardoso, R.P. Low-Temperature Plasma Nitrocarburizing of the AISI 420 Martensitic Stainless Steel: Microstructure and Process Kinetics. *Surf. Coat. Technol.* **2015**, *275*, 51–57. [CrossRef]

35. Alphonsa, J.; Raja, V.S.; Mukherjee, S. Study of Plasma Nitriding and Nitrocarburizing for Higher Corrosion Resistance and Hardness of 2205 Duplex Stainless Steel. *Corros. Sci.* **2015**, *100*, 121–132. [CrossRef]

36. Adachi, S.; Ueda, N. Combined Plasma Carburizing and Nitriding of Sprayed AISI 316L Steel Coating for Improved Wear Resistance. *Surf. Coat. Technol.* **2014**, *259*, 44–49. [CrossRef]

37. Fossati, A.; Borgioli, F.; Galvanetto, E.; Bacci, T. Corrosion Resistance Properties of Glow-Discharge Nitrided AISI 316L Austenitic Stainless Steel in NaCl Solutions. *Corros. Sci.* **2006**, *48*, 1513–1527. [CrossRef]